Available online at www.sciencedirect.com
SCIENCE DIRECT®
Journal of Power Sources 140 (2005) 319–330
JOURNAL OF POWER SOURCES
www.elsevier.com/locate/jpowsour

A hybrid neural network model for PEM fuel cells

Shaoduan Ou*, Luke E.K. Achenie

Department of Chemical Engineering, Unit 3222, 191 Auditorium Road, Storrs, CT 06269, USA

Received 22 July 2004; accepted 21 August 2004
Available online 27 October 2004

Abstract

The goal of this paper is to discuss a neural network modeling approach for developing a quantitatively good model for proton exchange membrane (PEM) fuel cells. Various ANN approaches have been tested; the back-propagation feed-forward networks and radial basis function networks show satisfactory performance with regard to cell voltage prediction. The effects of Pt loading on the performance of the PEM fuel cell have been specifically studied. The results show that the ANN model is capable of simulating these effects for which there are currently no valid fundamental models available from the open literature.

Two novel hybrid neural network models (multiplicative and additive), each consisting of an ANN component and a physical component, have been developed and compared with the full-blown ANN model. The results from the hybrid models demonstrate comparable performance (in terms of cell voltage predictions) compared to the ANN model. Additionally, the hybrid models show performance gains over the physical model alone. The additive hybrid model shows better accuracy than that of the multiplicative hybrid model in our tests.

Keywords: Artificial neural network; Proton exchange membrane fuel cell; Direct methanol fuel cell; Hybrid model; Back-propagation; Radial basis function

1. Introduction

A fuel cell is a device that can directly convert chemical energy to electric and thermal energy. Among various types of fuel cells, proton exchange membrane (PEM) fuel cells (also called polymer electrolyte membrane fuel cells) have attracted a significant amount of research interest in the past decade, especially in stationary and mobile power generators and electric vehicles. There are primarily two types of PEM fuel cells, namely the hydrogen PEM fuel cell and the direct methanol fuel cell (DMFC), both of which are efficient and clean replacements for conventional electricity generators.

Mathematical models are important tools for the design and optimization of fuel cells. In addition to the advances in PEM fuel cell design, many physical models have been developed to examine the complicated transport and electrochemical phenomena in hydrogen-feed PEM fuel cells [1–9] and DMFCs [10–15]. Unfortunately, several of these physical models are not accurate enough. Besides, physical models may not be available to describe input–output relations of interest, e.g., the effect of Pt loading, humidity, and other design or operating parameters on fuel cell performance.

A well-designed artificial neural network (ANN) model provides useful and reasonably accurate input–output relations because of its excellent multi-dimensional mapping capability. Artificial neural networks are computational paradigms made up of massively interconnected adaptive processing units, known as *neurons*. They have been extensively employed in various areas of science and technology, such as pattern recognition, signal processing and process control in engineering [16].

In this paper, we will examine the application of ANN approaches to the modeling of PEM fuel cells. Brief introductions to ANN, BP feed-forward, the RBF network and the formulation of the hybrid model will be given first. Next, construction of ANN and hybrid models will be described. The hybrid models employ an analytical model suitably modified to address the temperature effect. Finally, the results and conclusions will be discussed.

* Corresponding author. Tel.: +1 860 486 4600; fax: +1 860 486 2959.
E-mail address: shaoduan@engr.uconn.edu (S. Ou).

0378-7753/$ – see front matter © 2004 Elsevier B.V. All rights reserved.
doi:10.1016/j.jpowsour.2004.08.047

Nomenclature

a	slope parameter of sigmoid function
b	bias for a layer of ANN
D_i	diffusion coefficient of species i ($cm^2\ s^{-1}$)
D_i^{ref}	reference diffusion coefficient of species i ($cm^2\ s^{-1}$)
E	error function
F	Faraday's constant ($96\,488\ C\ eq^{-1}$)
h	radial basis function
i_0	exchange current density ($A\ cm^{-3}$)
i_0^{ref}	reference exchange current density ($A\ cm^{-3}$)
n	number of electrons transferred in the reaction
p	bias of hidden neurons
P	pressure
q	square of distance
R	universal gas constant ($8.3143\ J\ mol^{-1}\ K^{-1}$)
t	target for supervised training
$\vec{t}_j$	selected centers for RBF network
T	temperature (K)
T_{ref}	reference temperature (K)
w_j	weight of link j
x	input signal
$\vec{x}$	input vector
x_j	input from link j
y	output of a neuron
y_k	output of the kth neuron
Y	output of hybrid neural model
$Y_{additive}$	additive hybrid model
$Y_{analytical}$	analytical model
Y_{ANN}	artificial neural network model
$Y_{multiplicative}$	multiplicative hybrid model
z_i	output signal from the ith hidden layer to the kth neuron

Greek symbols

α	momentum term for Back-propagation training
η	learning rate
η_{oc}	open-circuit voltage (V)
η_{oc}^{ref}	reference open-circuit voltage (V)
φ	activation function
σ	proton conductivity ($\Omega^{-1}\ cm^{-1}$)
σ^{ref}	reference proton conductivity ($\Omega^{-1}\ cm^{-1}$)

2. Method formulation

2.1. Overview of ANN

ANN is a powerful data modeling tool that can be used to capture complex input/output relationships. There are many kinds of ANN models that have been developed for various applications. Based on the topology, the connection in an ANN can be feed-forward or feedback (recurrent). Unlike feedback networks, feed-forward networks do not contain any cycle in the connections between any two units. The learning of ANN can be supervised (learning with a teacher) or unsupervised (learning without a teacher) [17]. For supervised training, every input vector is associated with a target output vector that supervises the training process. For unsupervised training, the ANN model is not trained toward any specific target outputs; instead the ANN learns to recognize patterns in the input data.

The ANN has some significant features [17] including:

(1) nonlinearity,
(2) adaptivity,
(3) high parallelism,
(4) fault tolerance,
(5) uniformity of analysis and design and
(6) ability to tackle imprecise and fuzzy information.

These features make ANN a good tool for information processing.

In our study of ANN modeling for PEM fuel cells, we will focus on feed-forward neural networks with supervised training. A schematic diagram of a feed-forward artificial neural network is shown in Fig. 1. This network consists of an input layer, a hidden layer and an output layer. The output from a neuron in the hidden or output layer can be described by the following equation:

$$y = \varphi\left(\sum_{j=1}^{N} w_j x_j + b\right) \tag{1}$$

where the input signal x_j is multiplied by a weight. The bias b is then added to the weighted sum, and finally the output signal of the neuron is obtained by applying an activation function $\varphi(v)$ to the result. The most widely used activation function is the sigmoid function, a common form of which is defined by

$$\varphi(y) = \frac{1}{1 + e^{-ay}} \tag{2}$$

where a is the slope parameter. Given a network with one hidden layer, the input signal x_j for the neuron in the hidden layer comes directly from the value of input variable j. However, for a neuron in the output layer, the input signal x_j is the output from the jth neuron in the hidden layer. Considering a feed-forward network as shown in Fig. 1, the model equation for the entire neural network can be expressed as follows:

$$\begin{aligned} y_k &= \varphi\left(\sum_{i=1}^{K} w_{ki}^{o} z_i + b_2\right) \\ &= \varphi\left(\sum_{i=1}^{K} w_{ki}^{o} \varphi\left(\sum_{j=1}^{N} w_{ij}^{h} x_j + b_1\right) + b_2\right) \end{aligned} \tag{3}$$

where z_i is the output signal from the ith hidden neuron and y_k the output signal from the kth output neuron. The ANN in

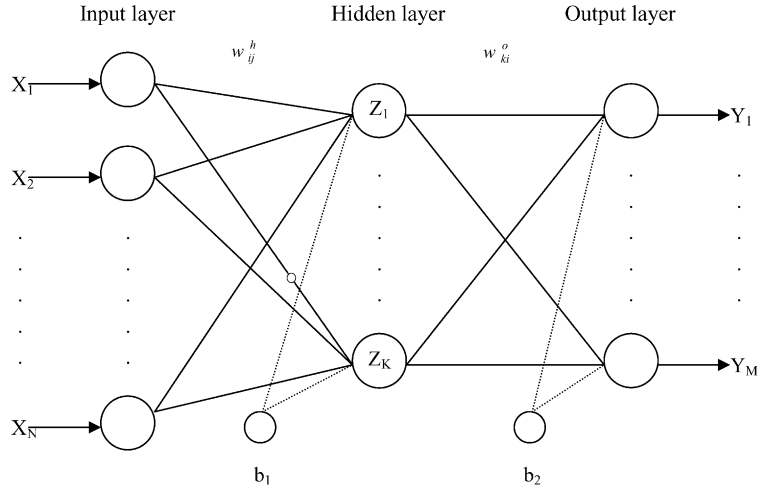

Fig. 1. The feed-forward multi-layer neural network with a single hidden layer.

Fig. 1 only contains one hidden layer. However, it is possible to have more than one hidden layer, as determined by the complexity of the problem. In our case studies, ANN models with one hidden layer were adequate for accurate prediction of output variables. The number of neurons in the input and output layers are related to the number of independent and dependent variables, respectively. The number of neurons in the hidden layer is related to the complexity of the problem. It is often obtained by trial and error during training.

2.2. Back-propagation feed-forward network

The back-propagation algorithm for training of ANNs was popularized by Rumelhart et al. in 1986 [18]. The learning (training) process adjusts the unknown network parameters (weights, bias, etc.) in order to minimize the least mean square error function defined as follows:

$$E(w) = \frac{1}{2}\sum_{j=1}^{N}\sum_{k=1}^{M}(t_k^j - y_k^j)^2 \tag{4}$$

where k refers to an output neuron, j is an index over the learning data, y_k^j the output of the network and t_k^j the corresponding target value. The weight adjustments are conducted by back-propagating the errors to the network. To accomplish this, the weight is adjusted by an amount proportional to the gradient of error with respect to the weight, shown as follows:

$$\Delta w = -\eta\frac{\partial E(w)}{\partial w} \tag{5}$$

where η is the learning-rate parameter and $\partial E(w)/\partial w$ the local gradient of $E(w)$ in Eq. (4). The BP algorithm performs better with a second-order term referred to as the momentum term α, which introduces the old weight change as a parameter for the computation of the new weight change.

$$\Delta w^{i+1} = -\eta\frac{\partial E(w)}{\partial w} + \alpha\,\Delta w^{i} \tag{6}$$

2.3. Radial basis function network

A radial basis function (RBF) network is a feed-forward network with a hidden layer that employs a nonlinear transformation from the input space to the hidden space. The hidden units implement a set of radial basis functions that constitute an arbitrary basis for the input vectors. Due to their excellent function approximation capabilities [19], RBF networks are often used for complex mapping. The model equation for an RBF network can be expressed as follows:

$$y_k(\vec{x}) = \varphi\left(\sum_{j=1}^{K} w_{ki}^{0} h(|\vec{x} - \vec{t}_j|,\, p_j) + b_k\right) \tag{7}$$

The structure of an RBF network is shown in Fig. 2. The hidden layer in RBF network is represented by a radial basis function $h(|\vec{x} - \vec{t}_j|,\, p_j)$, where $\vec{t}_j$ is the center that has to be selected a priori and p_j the bias for a given hidden neuron. The Gaussian function, as shown in Eq. (8), is widely used as the basis function for RBF networks:

$$h(q,\, p_j) = \mathrm{e}^{-p_j q} \tag{8}$$

where $q = |\vec{x} - \vec{t}_j|^2$.

Unlike a BP network that can have one or more hidden layers, an RBF network has only one hidden layer. The *delta rule*, which is commonly used in back-propagation feed-forward networks, is also used to update the weights of RBF networks during training.

2.4. Hybrid model development

In order to more accurately predict the performance of a PEM fuel cell in the case when physical models of limited accuracy are available, we propose a hybrid model that consists of an analytical component and an ANN component. The rationale behind this approach is to combine the part of the model that is well known from the physics of the problem,

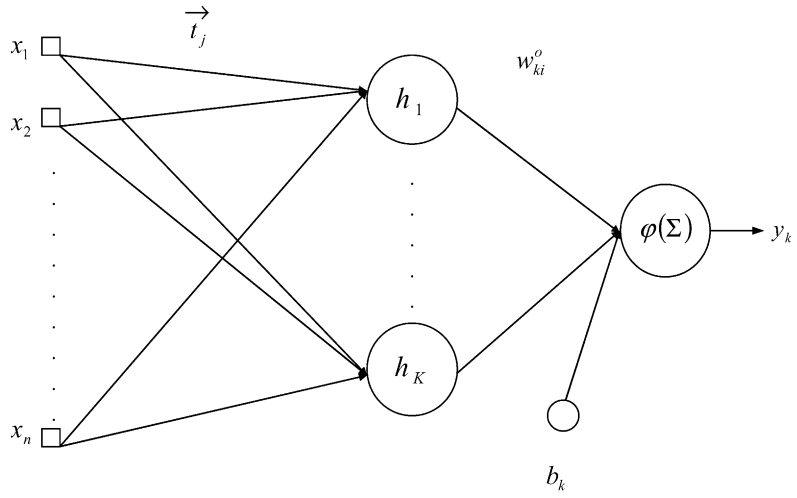

Fig. 2. Radial basis function network.

with the part that is poorly known but can be estimated quite effectively using neural networks.

The schematic of a multiplicative hybrid model is shown in Fig. 3. The cell voltage or other desired outputs can be described by a multiplicative model $Y_{\text{multiplicative}}(x_1, x_2, \ldots, x_N)$, which has an analytical component and an ANN component as follows:

$$Y = Y_{\text{multiplicative}}(x_1, x_2, \ldots, x_N) = Y_{\text{analytical}}(x_1, x_2, \ldots, x_N) Y_{\text{ANN}}(x_1, x_2, \ldots, x_N) \quad (9)$$

The vector $\vec{x} = [x_1, x_2, \ldots, x_N]$ represents operating or design variables. The function $Y_{\text{analytical}}(x_1, x_2, \ldots, x_N)$ is an analytical (physical) model that takes as input $\vec{x}$. The function $Y_{\text{ANN}}(x_1, x_2, \ldots, x_N)$ is an artificial neural network model that takes as input $\vec{x}$ and approximates the unmodeled parts in the physical model. Finally, the net prediction Y is the product of the predictions from $Y_{\text{analytical}}(x_1, x_2, \ldots, x_N)$ and $Y_{\text{ANN}}(x_1, x_2, \ldots, x_N)$. Similarly, an additive model can be constructed as

$$Y = Y_{\text{additive}}(x_1, x_2, \ldots) = Y_{\text{analytical}}(x_1, x_2, \ldots) + Y_{\text{ANN}}(x_1, x_2, \ldots) \quad (10)$$

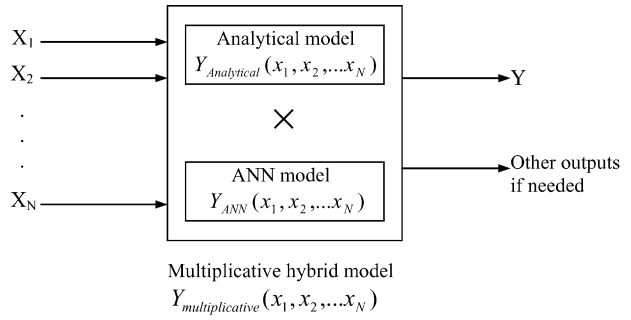

Fig. 3. The schematic of multiplicative hybrid model.

The analytical model used in the hybrid model is a one-dimensional model based on the model developed by Kulikovsky [14]. This original model was validated against the experimental data of a DMFC at a fixed operating temperature of 363 K. Using the method described in [10], we extended the capability of the original model to predict cell voltages under different operating temperatures. This is accomplished by approximating the temperature dependence of the material properties as summarized below.

2.5. Proton conductivity

$$\sigma = \sigma^{\text{ref}} \exp\left[1268\left(\frac{1}{T_{\text{ref}}} - \frac{1}{T}\right)\right] \quad (11)$$

This relationship [5] was used to correct the proton conductivity of Nafion for different temperatures, and was assumed valid for anode and cathode catalyst layers as well as the membrane.

2.6. Diffusion coefficients

The diffusion coefficients for the species in anode, cathode and MEA are assumed to have similar temperature dependence as the following [3]:

$$D_i = D_i^{\text{ref}} \exp\left[2436\left(\frac{1}{T_{\text{ref}}} - \frac{1}{T}\right)\right] \quad (12)$$

2.7. Dependence of i_0 on temperature

Anode:

$$i_{0,\text{an}} = i_{0,\text{an}}^{\text{ref}} \exp\left[8420\left(\frac{1}{T_{\text{ref}}} - \frac{1}{T}\right)\right] \quad (13)$$

Cathode [20]:

$$i_{0,\text{cat}} = i_{0,\text{cat}}^{\text{ref}} \exp\left[8804\left(\frac{1}{T_{\text{ref}}} - \frac{1}{T}\right)\right] \quad (14)$$

2.8. Open-circuit voltage

Open-circuit voltage was corrected for the thermodynamic effects of temperature and pressure by the following relationship:

$$\eta_{\text{oc}} = \eta_{\text{oc}}^{\text{ref}} + \Delta T\left(\frac{\partial E}{\partial T}\right) - \Delta N\frac{RT}{nF}\ln\left(\frac{P_2}{P_1}\right) \quad (15)$$

where $(\partial E/\partial T)$ is the gradient of electric potential over temperature. Liquid methanol solution was used as the anode feed in this study. For this system $(\partial E/\partial T) = -0.14\ \text{mV K}^{-1}$ and $\Delta N = -0.5$. All the reference parameters (at a reference temperature of 363 K) can be obtained from [14].

3. Development of ANN models and hybrid models

3.1. Preparation of data sets

Three data sets were assembled from experimental data in the open literature [21–23]. In addition, experimental data from the Connecticut Global Fuel Cell Center was used to test the ANN models. The cell performance data by Argyropoulos et al. [21] was obtained from a liquid-feed direct methanol fuel cell that was operated with methanol solution supplied at a rate of $1.12\,\text{cm}^3\,\text{min}^{-1}$ with air fed cathodes pressurized at 2 bar. The concentrations of methanol solution vary from 0.25 to 0.75 M. Cell operating temperatures vary from 303 to 363 K. Cell performance data by Gurau and Smotkin [22] is for a DMFC operated at temperatures between 313 and 353 K. Different concentrations of methanol solution (0.5, 1 and 2 M) and different MeOH solution flow rates (0.15, 0.5 and $5\,\text{ml}\,\text{min}^{-1}$) were used for each of their tests.

Data from Qi and Kaufman [23] were used to show the ability of the ANN model to simulate the effect of Pt loading on cell performance. Pt loading ($\text{mg}\,\text{cm}^{-2}$) is defined as the amount of Pt catalyst per area of the MEA. The tests were conducted on a hydrogen-feed PEM fuel cell under the cell temperature of 308 K. The hydrogen humidification temperature and air humidification temperature were 318 K. The stoichiometries of air and hydrogen were approximately 10 at a current density of $2.0\,\text{A}\,\text{cm}^{-2}$. Two experimental data sets from CGFCC were used to train and test ANN models. The first data set is the performance data for a liquid-feed DMFC operated at four different temperatures (303, 318, 333 and 348 K). The second data set examines the effects of operating temperature (313–353 K) and pressure (0.54–2.5 atm) on cell performance of a hydrogen-feed PEM fuel cell.

Each data set was separated into three parts, namely training data, test data and validation data. The training data was used to train the neural network to obtain the weights for the network. The test data were used to determine when training should be stopped. Finally, the validation data were employed to assess the performance of a trained neural network. Initially, the validation data are chosen depending on the desired number and form of outputs. The remaining data are separated into training and test data at a ratio of 3:1.

3.2. Constructing ANN

For BP feed-forward networks, a three-layer network (with one hidden layer) was found to be adequate for training. The architecture of the RBF network was the same as that of the three-layer feed-forward network. Generally speaking, input and output variables can be any process variables that are measurable (such as cell voltage, cell current density, cell temperature, relative humidity of air, etc.) during the operation of a fuel cell system. In our studies, input variables included cell temperature, concentration of methanol solution, methanol flow rate, current density, Pt loading and the ratio of the amount of Pt to carbon. The output variable chosen was the cell voltage.

The procedure to create a multiplicative hybrid model is illustrated in Fig. 4. From experimental data, we can obtain the input vector $\vec{x}$ and output vector Y. From the input vector, the analytical model can generate the simulated output vector $Y_{\text{analytical}}$. The ratio $Y/Y_{\text{analytical}}$ was obtained by dividing the output by the simulated cell voltages. Finally, the input vector and the ratio vector were used as the training data for the ANN model. The trained ANN model was combined with the analytical model to give predictions of output variables, corresponding to a given set of input variables. Therefore, the ratio $Y/Y_{\text{analytical}}$ or the difference $Y - Y_{\text{analytical}}$ of experimental cell voltages to those simulated by analytical model were used as target outputs for the hybrid model. The additive hybrid model can be similarly constructed as above. The final results were expressed as cell voltages by multiplying or adding the analytical part $Y_{\text{analytical}}$ to the output obtained from the ANN model.

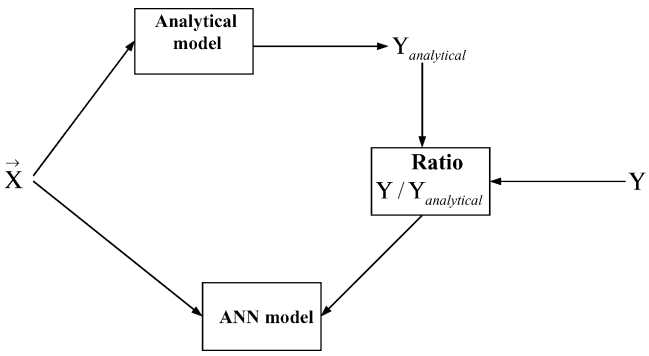

Fig. 4. Constructing the multiplicative hybrid model.

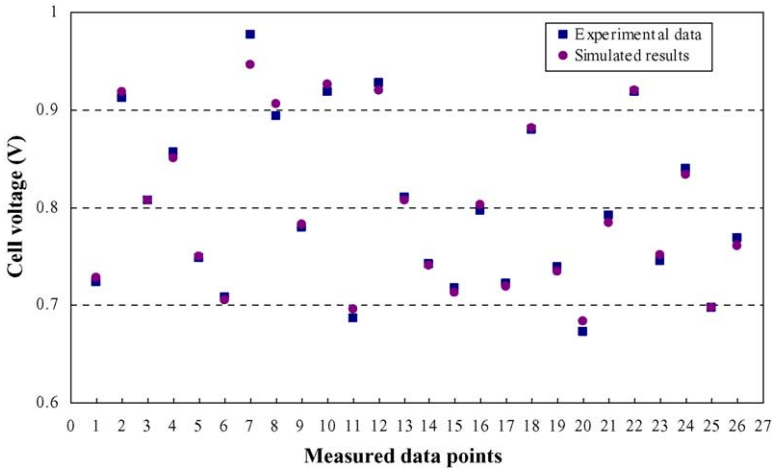

Fig. 5. Comparison of simulated cell voltages and experimental data for a PEM fuel cell.

The number of hidden neurons in the hidden layer can vary, and will affect the quality of the ANN. Therefore, an optimal number of hidden neurons need to be determined for each neural network to achieve the best performance. This was done by trial and error.

3.3. Training, testing and validating ANN

Training of an ANN model is the process of adjusting the weights of links among the neurons. The weights are updated after processing each example (incremental training) or after processing the whole training data set (batch training). During training, the error function is reduced as the number of training epoch increases. Testing data set is used to determine when to stop training process by monitoring the error of the test data. The error from the test data is usually less than that from the training data. If the two error quantities become equal, we need to stop the training to make sure the network is not over-trained. Once the ANN is trained, the model is ready to give predictions of output variables. The simulated outputs are then compared to the experimental ones in the validated data set to assess the performance of the ANN model.

4. Results and discussion

Fig. 5 shows the comparison of simulated cell voltages from ANN model to experimental results. We employed the data set from a hydrogen-feed PEM fuel cell at CGFCC. The simulated values of the cell voltage (the outputs of the ANN model) were obtained through the ANN model, based on the three input variables, namely current density, concentration and flow rate of the methanol solution. Each data point from the simulation in Fig. 5 represents an output from the ANN model, corresponding to a certain set of the input variables described above. We see that the results from the ANN model are in good agreement with the experimental ones. However, there are large errors between simulated and experimental values at the high cell voltage (i.e. close to the open-circuit voltage). The same observations were made in our tests with

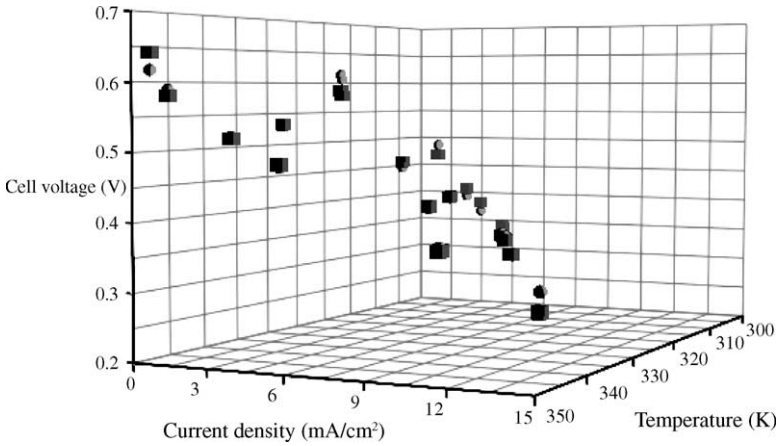

Fig. 6. Comparison of ANN simulation to experimental data from the DMFC by CGFCC: (cubes) experimental data; (spheres) simulated results.

Table 1
Data table for Fig. 6

Temperature (K)	Current density (mA cm^{-2})	Experimental data (V)	Simulated results (V)
303	2.928	0.4103	0.3972
318	5.295	0.4127	0.4102
318	7.662	0.3468	0.3529
303	4.599	0.3468	0.3416
333	7.649	0.4151	0.4123
303	3.599	0.3858	0.3718
348	5.38	0.486	0.4823
333	1.549	0.5348	0.5349
348	0.1952	0.6422	0.6175
348	0.9394	0.5812	0.5888
303	4.648	0.3419	0.3403
318	7.71	0.3443	0.3517
333	10.88	0.3492	0.3503
348	14.82	0.3028	0.3297
318	3.172	0.4689	0.4594
348	11.32	0.3761	0.3798
348	3.489	0.5201	0.5223
318	0.3172	0.5861	0.6137
303	1.525	0.4713	0.4885
318	7.552	0.3516	0.3555
318	0.3782	0.5788	0.6067

other data sets. The main reason for this disparity could be that there were not sufficient experimental data points tracking the rapidly decreasing cell voltage in this activation polarization region, and thus the ANN model did not have sufficient information to make good predictions for data points in that region. Possible ways to solve this problem are:

1. Making more measurements in the activation polarization region during the experimental phase.
2. Approximating the values on the performance curve, and adding the values to the data set, when additional experiments are difficult to be conducted.

With experimental data from a DMFC, an ANN model was trained. The results generated by the model were then compared to the experimental data. Since only two input variables were used (temperature and current density) in this model, the results can be visualized in a three-dimensional space, as shown in Fig. 6. The cubes in the plot represent experimental results, and the spheres represent simulated results from ANN model. Again, we see that the simulated results show good agreement with experimental results. The comparison of experimental and simulated results is shown more clearly in Table 1. Fig. 7 displays the simulated polarization and power density curves for the PEM fuel cell operated under 1 and 2 atm (333 K).

Table 2
Errors in the tests

Data set used	MSE (10^{-3})
Fig. 6	0.074
Fig. 7	0.24
Fig. 8	0.083
Fig. 9	
BP	1.50
BP with momentum term	1.00
RBF	1.40
Fig. 10	0.13
Fig. 14	
Analytical model	3.03
ANN	0.48
Multiplicative	0.45
Additive	0.34

Fig. 8 demonstrates the performance comparison of different ANN approaches. We conclude that the results from BP with momentum term match the experimental results better than those from the other approaches. The errors from all the approaches tested are listed in Table 2. We see that the performance of the RBF approach is also fairly good. In other tests and by comparisons with other data sets, it is found that the performance of BP with momentum term is superior over other approaches. Therefore, if not specifically mentioned, it is assumed that the BP with momentum term is employed in the other ANN models in this paper.

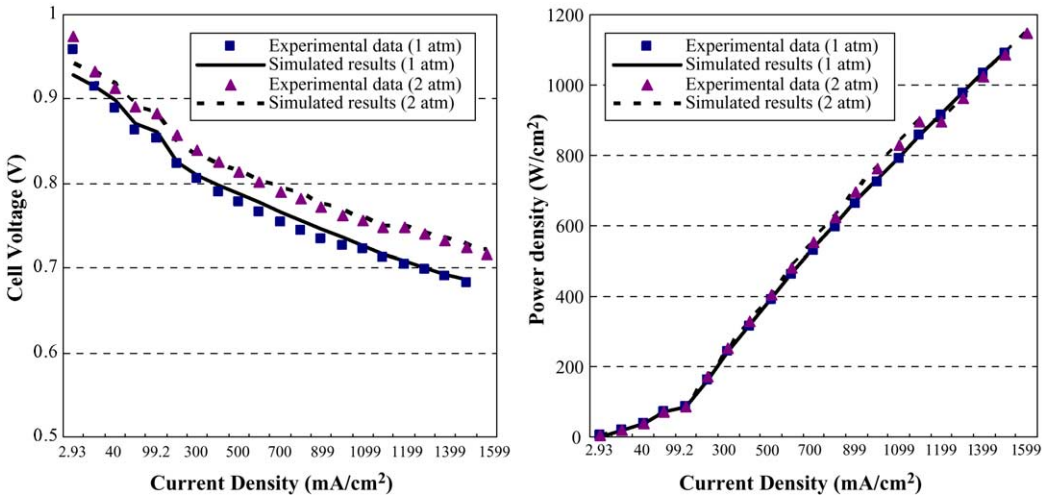

Fig. 7. Comparison of simulated results and experimental data of a PEM fuel cell by CGFCC (operating temperature: 333 K).

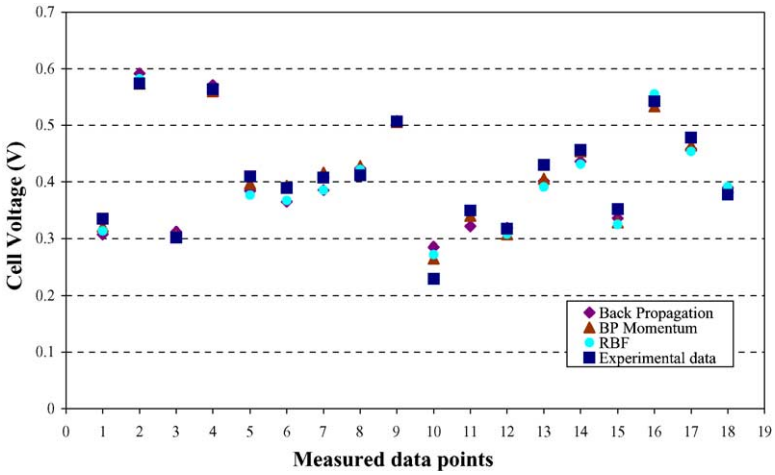

Fig. 8. Comparison of different ANN approaches.

Fig. 9 shows the ANN prediction of the performance of a hydrogen-feed PEM fuel cell with different Pt loadings. Four input variables including current density, temperature, Pt/C of the catalyst and catalyst loading are considered. The simulated results by ANN model nicely agree with the experimental data. Therefore, the ANN model can be very helpful when the effect of Pt loading is needed for further analysis of a fuel cell system. Fig. 10 displays the simulated polarization curves for PEM fuel cells with four different Pt loadings. We observe from Fig. 10 that for a PEM fuel cell operated under 308 K and with Pt/C of 0.2, better cell performance can be obtained with increasing Pt loading from 0.05 to 0.3. This conclusion is consistent with the experimental results by Qi and Kaufman [23]. We expect that ANN models to be equally good for the prediction of the effects of other factors (such as relative humidity) in the PEM fuel cell systems.

To set up the hybrid models, the original analytical model (fixed at 363 K) [14] was validated against experimental data [21] as shown in Fig. 11. The results simulated by this model agree with the results given in Kulikovsky [14]. Fig. 12 shows the comparison of experimental data and results from the model we have modified to account for the temperature effect on cell performance. We see that the modified model can provide fairly good predictions for the cell voltages under various operating temperatures. Figs. 13 and 14 compare the performance of hybrid models, with the pure ANN model and the pure analytical model. The performances of both hybrid models are much better than that of the analytical model. This is due to the limitation of many currently available physical models. Specifically, to fit experimental data, a certain number of parameters of a physical model have to be adjusted beforehand. After validation, those parameters are fixed. Therefore, when new operating conditions are applied, the physical model usually cannot offer quantitatively good predictions without another round of parameter adjustment. The multiplicative model shows slightly better predictions than the ANN model. On the other hand, there is a great improvement in accuracy in the additive model (in terms of MSE comparisons listed in Table 2). The reason for the performance improvement in the hybrid model is that by design, the ANN component only tackles the theoretically unknown parts, while the other parts are already addressed by the phys-

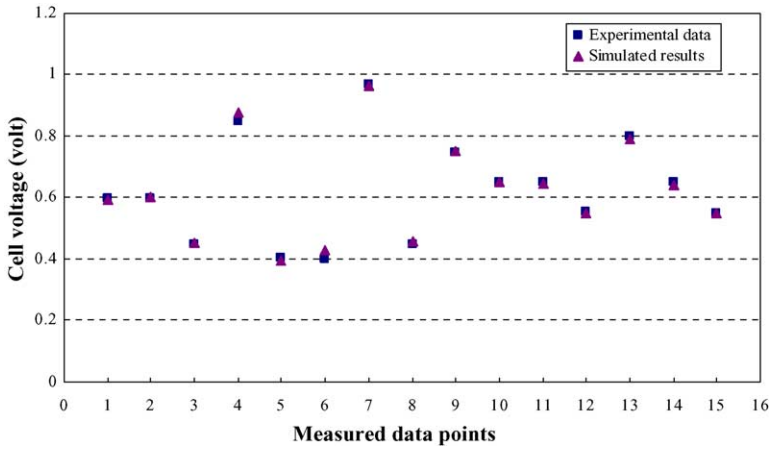

Fig. 9. ANN modeling of the Pt loading effect on cell voltage.

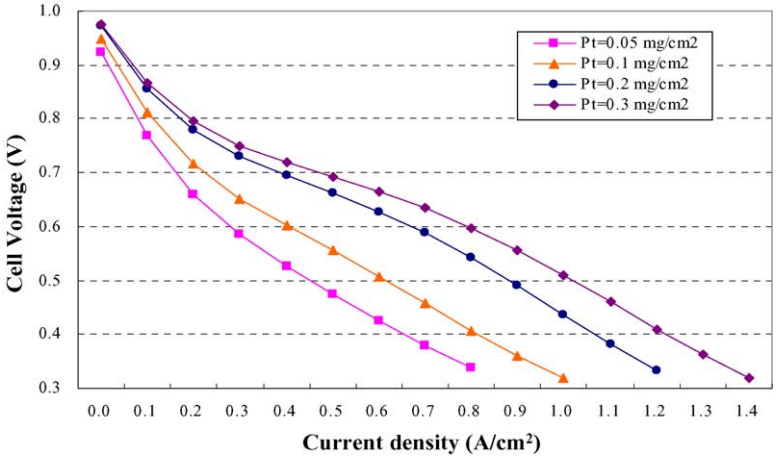

Fig. 10. Simulated performance curve for the PEM fuel cell with various Pt loadings (temperature: 308 K, Pt/C: 0.2).

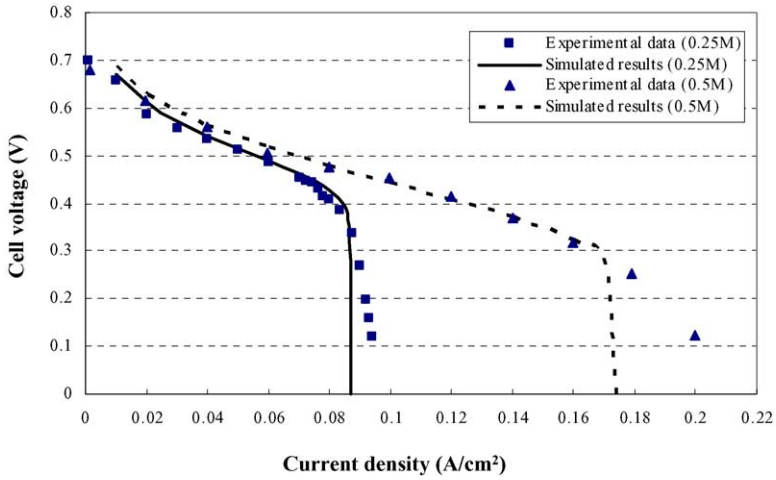

Fig. 11. Model validation for DMFC operated at 363 K.

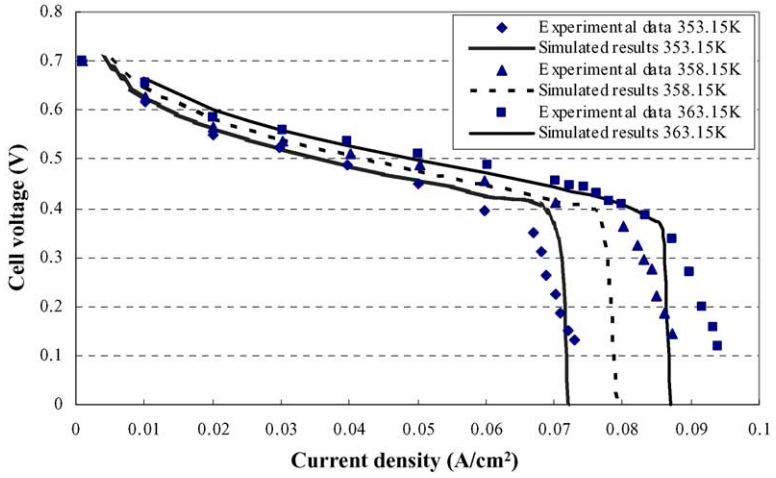

Fig. 12. Model validation for DMFC operating at different temperatures (C_{MeOH}: 0.25 M).

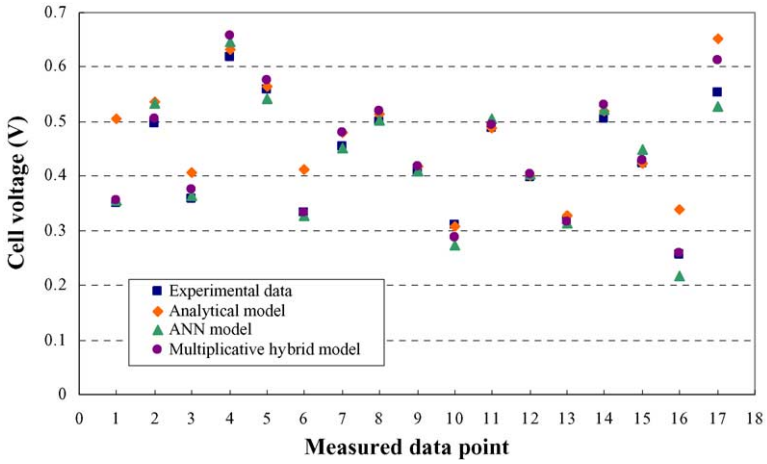

Fig. 13. Comparison of multiplicative hybrid model to ANN model, analytical model and experimental data.

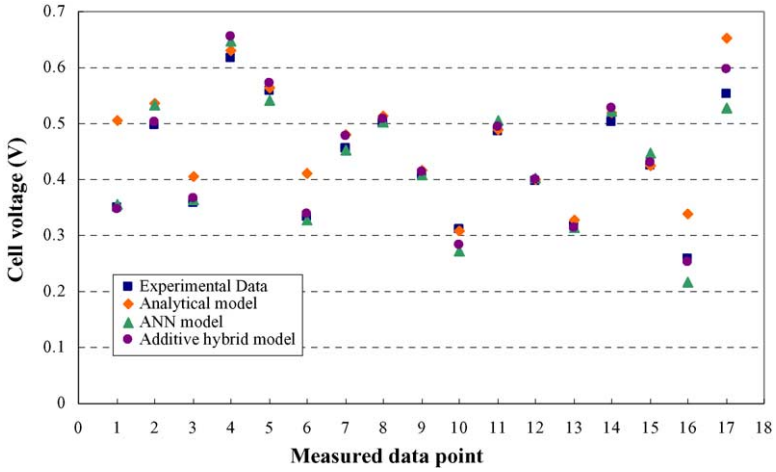

Fig. 14. Comparison of additive hybrid model to ANN model, analytical model and experimental data.

ical component. However, in a pure ANN model, the various scales of the fuel cell system have to be handled by a single ANN model. This means that to achieve equivalent accuracy with hybrid models, the pure ANN model needs to be trained with significantly more data points. In our case, the experimental data are sufficient to train an ANN model with good accuracy in the prediction of cell voltage. In the cases when a well-trained ANN model cannot be obtained because of inadequate experimental data, we expect greater improvement in the performance by the hybrid model over the ANN model.

5. Conclusions

The ANN approach was employed in the modeling of PEM fuel cells, and has shown good performance in the prediction of cell voltages. Specifically, we have been able to model the effect of Pt loading on cell voltage. The time required for training an ANN is not much different from the time needed to set up a physical model. However, the trained ANN model is computationally fast and easy to use, and therefore suitable for multi-dimensional mapping applications in fuel cell systems, especially in the cases where physical models are not readily available. Among various methods of ANN, we have tested two widely used approaches, namely BP feed-forward network and RBF network. Both of them were able to offer good approximations on cell voltages.

Hybrid models that combine a physical model with an ANN model were constructed. The motivation is that accuracies in the physical model can be compensated by the ANN model, which has good accuracy in multi-dimensional mapping. In our tests, both additive and multiplicative hybrid models showed much better performance than the analytical model alone, especially the additive hybrid model. The hybrid model also demonstrated modest improvement in accuracy, compared to the pure ANN.

Acknowledgements

The authors would like to acknowledge the Connecticut Global Fuel Cell Center for providing financial support, and

Dr. Raymond England and Hui Xu for providing experimental data.

Appendix A. Analytical model for the hybrid model

The model used for the analytical component of the hybrid model is a one-dimensional analytical model developed by Kulikovsky [14]. It was validated against experimental data [21] of a liquid-feed DMFC operated at 363.15 K. The model was extended to include the temperature dependence by the method used in [10] and described earlier in this paper.

The simplified fitting equations for the calculation of cell voltage are summarized here, and the procedures and methods to derive these equations can be found in [14]. The overall cell voltage is written as

$$V_{\text{cell}} = \eta_{\text{oc}} - \eta_{\text{a}} - \eta_{\text{c}} - \eta_{\text{ohmic}} \tag{A.1}$$

The ohmic overpotential is calculated by

$$\eta_{\text{ohmic}} = \frac{j_0 l_{\text{m}}}{\sigma_{\text{m}}} \tag{A.2}$$

Anode and cathode overpotentials are described by

$$\eta_{\text{a}} = \eta_{\text{a},0}\left[\phi\left(\frac{j_0}{j_{\text{a}}}\right)\ln\left(\frac{j_0}{j_{\text{a}}}\right) - \ln k^{\text{a}} - \gamma^{\text{a}}\ln\left(1 - \frac{j_0}{j_{\text{a,lim}}}\right) + \gamma^{\text{a}}\ln\left(1 + \beta + n_{\text{d}}\frac{j_0}{j_{\text{w}}}\right)\right] \tag{A.3}$$

$$\eta_{\text{c}} = \eta_{\text{c},0}\left[\phi\left(\frac{j_0}{j_{\text{c}}}\right)\ln\left(\frac{j_0}{j_{\text{c}}}\right) - \ln k^{\text{c}} - \gamma^{\text{c}}\ln\left(1 - \frac{j_0}{j_{\text{c,lim}}} - r_{\text{cross}}\right)\right] \tag{A.4}$$

Here

$$\phi(x) = 1 + \frac{x}{1+x} \tag{A.5}$$

$$\eta_{\text{a},0} = \frac{RT}{\alpha_{\text{a}}F} \tag{A.6}$$

$$j_{\text{a}} = \frac{2\sigma_{\text{a,cl}}\eta_{\text{a},0}}{l_{\text{a,cl}}} \tag{A.7}$$

$$k^{\text{a}} = \frac{l_{\text{a,cl}} i_{\text{a}}}{j_{\text{a}}}\left(\frac{C_{\text{a}}}{C_{\text{a,ref}}}\right)^{\gamma_{\text{a}}} \tag{A.8}$$

$$\eta_{\text{c},0} = \frac{RT}{\alpha_{\text{c}}F} \tag{A.9}$$

$$j_{\text{c}} = \frac{2\sigma_{\text{c,cl}}\eta_{\text{c},0}}{l_{\text{c,cl}}} \tag{A.10}$$

$$k^{\text{c}} = \frac{l_{\text{c,cl}} i_{\text{c}}}{j_{\text{c}}}\left(\frac{C_{\text{c}}}{C_{\text{c,ref}}}\right)^{\gamma_{\text{c}}} \tag{A.11}$$

$$\beta = \frac{D_{\text{m}} l_{\text{a,dl}}}{D_{\text{a,dl}} l_{\text{m}}} \tag{A.12}$$

$$j_{\text{w}} = F\frac{D_{\text{a,dl}} W_{\text{H}_2\text{O}}}{l_{\text{a,dl}}} \tag{A.13}$$

$$j_{\text{a,lim}} = 6F\frac{D_{\text{a,dl}} C_{\text{a}}}{l_{\text{a,dl}}} \tag{A.14}$$

$$r_{\text{cross}} = \frac{j_{\text{a,lim}}}{j_{\text{c,lim}}}\left(\frac{\beta + n_{\text{d}}(j_0/j_{\text{w}})}{1 + \beta + n_{\text{d}}(j_0/j_{\text{w}})}\right)\left(1 - \frac{j_0}{j_{\text{w}}}\right) \tag{A.15}$$

$$j_{\text{c,lim}} = 4F\frac{D_{\text{c,dl}} C_{\text{c}}}{l_{\text{c,dl}}} \tag{A.16}$$

References

[1] D.M. Bernardi, M.W. Verbrugge, Mathematical model of a gas diffusion electrode bonded to a polymer electrolyte, AIChE J. 37 (1991) 1151.

[2] D.M. Bernardi, M.W. Verbrugge, A mathematical model of the solid–polymer–electrolyte fuel cell, J. Electrochem. Soc. 139 (1992) 2477.

[3] T.E. Springer, T.A. Zawodinski, S. Gottesfeld, Polymer electrolyte fuel cell model, J. Electrochem. Soc. 138 (1991) 2334.

[4] T.E. Springer, M.S. Wilson, S. Gottesfeld, Modeling and experimental diagnostics in polymer electrolyte fuel cells, J. Electrochem. Soc. 140 (1993) 3513.

[5] T.V. Nguyen, R.E. White, A water and heat management model for proton-exchange-membrane fuel cells, J. Electrochem. Soc. 140 (1993) 2178.

[6] J.S. Yi, T.V. Nguyen, An along-the-channel model for proton exchange membrane fuel cells, J. Electrochem. Soc. 145 (1998) 1149.

[7] J.S. Yi, T.V. Nguyen, Multicomponent transport in porous electrodes of proton exchange membrane fuel cells using the interdigitated gas distributors, J. Electrochem. Soc. 146 (1999) 38.

[8] S. Um, C.Y. Wang, K.S. Chen, Computational fluid modeling of proton exchange membrane fuel cells, J. Electrochem. Soc. 147 (2000) 12.

[9] Z.H. Wang, C.Y. Wang, K.S. Chen, Two-phase flow and transport in the air cathode of proton exchange membrane fuel cells, J. Power Sources 94 (1) (2001) 40.

[10] K. Scott, W. Taama, J. Cruickshank, Performance and modeling of a direct methanol solid polymer electrolyte fuel cell, J. Power Sources 65 (1997) 159.

[11] S.F. Baxter, V.S. Battaglia, R.E. White, Methanol fuel cell model: anode, J. Electrochem. Soc. 146 (2) (1999) 437.

[12] A.A. Kulikovsky, J. Divisek, A.A. Kornyshev, Two-dimensional simulation of direct methanol fuel cell: a new (embedded) type of current collector, J. Electrochem. Soc. 147 (2000) 953.

[13] A.A. Kulikovsky, Two-dimensional numerical modeling of a direct methanol fuel cell, J. Appl. Electrochem. 30 (2000) 1005.

[14] A.A. Kulikovsky, The voltage–current curve of a direct methanol fuel cell: "exact" and fitting equations, Electrochem. Commun. 4 (2002) 939.

[15] Z.H. Wang, C.Y. Wang, Mathematical modeling of liquid-feed direct methanol fuel cells, J. Electrochem. Soc. 150 (4) (2003) 508.

[16] P.K. Simpson, Institute of Electrical and Electronics Engineers, Neural Networks Applications, Institute of Electrical and Electronics Engineers, New York, 1996.

[17] S.S. Haykin, Neural Networks: A Comprehensive Foundation, Prentice Hall, Upper Saddle River, NJ, 1999.

[18] D.E. Rumelhart, G.E. Hinton, R.J. Williams, Learning representations by back-propagating errors, Nature 323 (1986) 533.

[19] J. Park, J.W. Sandberg, Universal approximation using radial basis functions network, Neural Comput. 3 (1991) 246.

[20] A. Parthasarathy, S. Srinivasan, A.J. Appleby, C.R. Martin, Temperature dependence of the electrode kinetics of oxygen reduction at the platinum/Nafion interface – a microelectrode investigation, J. Electrochem. Soc. 139 (1992) 2530.
[21] P. Argyropoulos, K. Scott, A.K. Shukla, C. Jackson, Empirical model equations for the direct methanol fuel cell, Fuel Cells 2 (2002) 78.
[22] B. Gurau, E.S. Smotkin, Methanol crossover in direct methanol fuel cells: a link between power and energy density, J. Power Sources 112 (2002) 339.
[23] Z. Qi, A. Kaufman, Low Pt loading high performance cathodes for PEM fuel cells, J. Power Sources 113 (2003) 37.